Chemical Engineering Journal 493 (2024) 152559

Contents lists available at ScienceDirect

Chemical Engineering Journal

journal homepage: www.elsevier.com/locate/cej

Phosphate-based ionic liquids for advanced interface modification in perovskite photovoltaics: Novel insights for ionic liquid molecule design

Guo Yang [a,1], Fei Wang [a,b,1], Chao Zhou [a,1], Yonggui Sun [a,1], Taomiao Wang [a], Qiannan Li [a], Yongjun Li [a], Xiao Liang [a,b], Xianfang Zhou [a,b], Quanyao Zhu [b], Haoran Lin [a], Hanlin Hu [a,*]

[a] Hoffmann Institute of Advanced Materials, Shenzhen Polytechnic University, 7098 Liuxian Boulevard, Shenzhen 518055, China
[b] State Key Laboratory of Advanced Technology for Materials Synthesis and Processing, School of Materials Science and Engineering, Wuhan University of Technology, Wuhan, China

ARTICLE INFO

Keywords:
Interface modification
Ionic liquid
Perovskite solar cells
Stability

ABSTRACT

Interface modification stands out as a crucial method to enhance the performance of perovskite solar cells. This study explores the utilization of the ionic liquid 1-Methyl-3-propylimidazolium phosphate (MPIMPH), containing phosphate (PO_4^{3-}) groups, as a modifier for SnO_2/perovskite interfaces. Detailed investigations delve into the specific impact of IL MPIMPH on defects in tin dioxide, perovskite defects, perovskite crystallization, morphology, and overall device performance. Initially, Density Functional Theory (DFT) is employed to evaluate the defect passivation potential of different anions on tin vacancies within the SnO_2 matrix, revealing the exceptional defect passivation ability of the PO_4^{3-} group. Chemical interactions between ILs MPIMPH and SnO_2, as well as perovskite, are confirmed, establishing a fundamental basis for interface defect passivation. ILs-based interface modification enhances interface contact, influencing the lead iodide conversion into perovskite and perovskite crystallization, ultimately leading to the formation of high-quality perovskite thin films. ILs also effectively suppress interfacial charge recombination and optimize the energy alignment of the SnO_2/perovskite interface to enhance carrier extraction. Benefiting from the interface modification with ILs, the optimized device achieved an impressive device efficiency of 24.24 % with remarkable durability. This work provides an novel aspect for designing ionic liquids to enhance interface modification, contributing to upscaling and application of perovskite photovoltaics.

1. Introduction

Perovskite solar cells (PSCs) have emerged as a prospective photovoltaic (PV) technology for the production of renewable energy [1–5]. Capitalizing on their remarkable attributes, including their robust light absorption, extensive carrier diffusion length, and minimal exciton binding energy, PSCs have witnessed an extraordinary surge in their power conversion efficiency (PCE), soaring from 3.8 % to 26.1 % over the span of a decade [6]. During the continuous breakthroughs in the field of PSCs, the updating of electron transport layer materials and the modification of the electron transport layer (ETL)/perovskite interface assume pivotal roles. The selection of ETL materials and the precise interaction between the ETL and the perovskite layer will have a direct impact on the crystallization process, the overall film quality of the perovskite and extraction of interface charges [7–9].

Titanium dioxide (TiO_2) has been extensively employed as conventional ETL material in the creation of effective and enduring perovskite devices [10–12]. Nonetheless, the demanding manufacturing conditions and the deterioration of device stability, stemming from its elevated processing temperatures and limited UV stability, act as obstacles to its continued progress [13]. These challenges are particularly pronounced in the context of flexible and large-area PSCs advancement. Emerging as a highly viable substitute for TiO_2, tin dioxide (SnO_2) boasts enhanced bulk electron mobility, more moderate processing temperatures, and diminished photocatalytic reactivity, which further released the potential of PSCs [14–16]. Surprisingly, solar cells employing SnO_2 as the electron transport layer, which is based on a straightforward and convenient fabrication approach, have achieved an efficiency exceeding 25.5 % [17]. However, the tin oxide defects easily generated during the processing of tin and oxygen vacancies adversely affect the electron

* Corresponding author.
E-mail address: hanlinhu@szpu.edu.cn (H. Hu).
[1] G. Y., F. W., C. Z. and Y. S contributed equally to this work.

https://doi.org/10.1016/j.cej.2024.152559
Received 14 March 2024; Received in revised form 23 May 2024; Accepted 25 May 2024
Available online 25 May 2024

transfer and the charge recombination, thereby impeding the further enhancement of perovskite devices based on SnO_2 [18–20]. Moreover, it is essential to optimize the direct surface contact between the tin dioxide layer and the perovskite layer in order to guarantee a perovskite growth environment with a high-quality morphology. To tackle the issues mentioned above, an array of materials, including organic salts, inorganic salts, polymers, ionic liquids (ILs), and metal frameworks, are utilized as interface modifiers for the SnO_2/perovskite [21–24]. Simultaneously, they regulate the defects in SnO_2 and perovskite, leading to the attainment of high-quality thin films and the optimization of photovoltaic performance in devices [25,26]. Among the array of materials, ILs shine for their eco-friendly attributes, thermal resilience, chemical durability, varied molecular structures, and potent chemical affinities toward both perovskite and tin dioxide [9,27–29]. These valuable characteristics have spurred the extensive integration of ILs as interface modifiers for the SnO_2/perovskite interface. Chen and colleagues reported an IL, imidazolium tetrafluoroborate ($IMBF_4$) as efficient SnO_2/perovskite interfacial modifier to achieve a champion efficiency 23.05 % [30]. The BF_4^- in IL $IMBF_4$ can fill oxygen vacancies through formation of the strong coordination bond between BF_4^- with Sn^{2+} and the cation IM^+ simultaneously passivating the uncoordinated Pb^{2+} for the effective suppression of vacancy defect in perovskite, leading to the more efficient charge transfer. Mu and colleagues incorporate the IL formamidine acetate (FAAc) at the SnO_2/perovskite interface, achieving simultaneous passivation of defects on both the SnO_2 electron transport layer (ETL) surface and the bottom of the perovskite layer [31]. Through the proficient passivation of interface defects by FAAc, the recombination of interfacial charges is efficiently alleviated, leading to a remarkable amplification in the filling factor to around 0.83 and elevates the PCE to 23.05 %. Nonetheless, present-day research predominantly centers on singular and prevalent ILs encompassing BF_4^-, AC^-, I^-, Cl^-, and Br^- as candidates for interface modification. The examination of distinct anions featuring diverse chemical structures, aiming to elucidate their precise contributions to the underpinning principles governing IL structure design in the context of interface modification, and the pursuit of innovative ILs with markedly enhanced efficacy for interface modification, continues to be encumbered by inherent challenges.

In this work, we employed IL 1-Methyl-3-propylimidazolium phosphate (MPIMPH) with phosphate (PO_4^{3-}) groups as agents to modify SnO_2/perovskite interfaces. We extensively investigated the specific effects of IL MPIMPH on tin dioxide defects, perovskite defects, perovskite crystallization, morphology, and overall device performance have been extensively investigated. Initial Density functional theory (DFT) calculations comprehensively compared the defect passivation abilities of various anions on tin vacancies in SnO_2, revealing that among the numerous common anions, the PO_4^{3-} group exhibited the highest defect passivation capability. We validated strong chemical interactions between IL MPIMPH and both SnO_2 and perovskite through infrared spectroscopy (FTIR), nuclear magnetic resonance (NMR), and X-ray photoelectron spectroscopy (XPS), forming a foundational basis for passivating interface defects. Furthermore, MPIMPH IL modification of the interface enhances the interface contact, thereby influencing the degree of lead iodide transformation to perovskite and the crystallization of perovskite. This leads to the creation of high-quality perovskite thin films characterized by substantial and consistent grain sizes, supported by data from grazing-incidence wide-angle scattering measurements (GIWAXS), atomic force microscopy (AFM), and scanning electron microscopy (SEM). Capitalizing on the interface modification facilitated by MPIMPH ILs, perovskite materials treated with IL exhibited reduced charge recombination, extended photoluminescence lifetime, and enhanced carrier transport efficiency. Consequently, ILs-treated PSCs achieved a remarkable PCE of 24.24 %, demonstrating a substantial improvement over the reference device's efficiency of 22.60 %.

2. Results and discussion

The planar PSCs device was fabricated using a structure of ITO/SnO_2/perovskite/Spiro-OMeTAD/Au, following our previously reported method [32]. Detailed fabrication steps can be found in the experimental section. In this study, we employed an ILs, MPIMPH, composed of cations containing imidazole groups and anions consisting of phosphate (Fig. S1), to modify the SnO_2/perovskite interface in the planar PSCs device. The IL's cations were deliberately selected for their strong chemical interactions between imidazole groups and perovskite constituents, known for their remarkable capability in defect passivation and ion migration inhibition in PSCs field [29,33]. The cations encompass fragments with imidazole groups due to their effective interaction with perovskite material. The anionic phosphate group, containing the P═O moiety, has been verified to exhibit potent defect passivation effects on SnO_2, effectively enhancing the charge transfer at the interface [34–36]. Fig. 1a schematically depicts the distinct chemical interaction between the ILs MPIMPH with both perovskite and SnO_2 layers. The interaction between the imidazole groups of the IL cations and the perovskite is anticipated to lead to the passivation of Pb-I antisite defects on the bottom surface of perovskite films. Concurrently, the anions are expected to coordinate with Sn^{4+} within the SnO_2 film, contributing to the mending of oxygen vacancy deficiencies within the electron transport layer.

To substantiate specific chemical interactions, XPS analysis was conducted on SnO_2 films, comparing instances with and without ILs MPIMPH modification. Two distinct peaks at 495.45 and 487.04 eV in the Sn 3d spectrum for control SnO_2 sample, correspond to Sn $3d_{3/2}$ and $3d_{5/2}$, respectively. After ILs MPIMPH modification of, the binding energies of Sn $3d_{3/2}$ and Sn $3d_{5/2}$ were decreased to 495.12 and 486.77 eV, indicating strong coordination interaction of PO_4^{3-} in MPIMPH with Sn^{4+} in SnO_2. In Fig. 1c, the O 1s peaks of control and ILs-modified SnO_2 films were deconvoluted into two peaks of 531.99 eV and 530.42 eV, attributed to the lattice oxygen and vacancy oxygen in SnO_2 [37], respectively. The additional signal peak after ILs modification is attributed to the phosphate group, indicating the ILs attachment to the surface of SnO_2. The proportion of vacancy oxygen decreases from 0.5 to 0.3 after ILs MPIMPH modification (Fig. 1d), as calculated through the previously reported formula [38]. This promotes the reduction of defect-assisted photo-generated carrier trapping and enhances the efficiency of electron extraction [39]. Subsequently, relevant device structures were supplemented to explore the specific effects of IL modification on the conductivity and electron mobility of tin dioxide. *J-V* curves of devices were obtained *via* the structure of ITO/Ag/SnO_2 or MPIMPH-SnO_2/Ag to evaluate the conductivity of SnO_2 or MPIMPH-SnO_2 films. The conductivity can be determined from the formula $I = \sigma AL^{-1} V$ [40], where A and L represent the active area and thickness, respectively. As displayed in Fig. S2a, the electron conductivity of the MPIMPH-SnO_2 film (9×10^{-3} mS*cm^{-1}) is slightly higher than that of the SnO_2 film (2.5×10^{-3} mS*cm^{-1}). To reveal the role of MPIMPH modification in the electronic and interfacial characteristics, Fig. S2b demonstrates the Mott − Gurney $J^{1/2}$-V curves of devices with a structure of ITO/Ag/SnO_2 or MPIMPH-SnO_2/Ag based on the space charge limited current (SCLC) method [41]. The mobility of electrons can be determined from the Mott–Gurney law ($J_D = 9\mu\varepsilon\varepsilon_0 V^2/8L^3$) [42]. The calculated electron mobility of MPIMPH-SnO_2 film (2.225×10^{-3} cm^2 V^{-1} s^{-1}) is significantly higher in comparison with that of the SnO_2 film (3.585×10^{-4} cm^2 V^{-1} s^{-1}), which will benefit to accelerate the electron transport. These results confirm that the SnO_2 modification can facilitate charge transport. In order to delve deeper into the chemical interactions between ILs and SnO_2, FTIR spectroscopy was conducted for the MPIMPH and MPMPH + SnO_2 samples. The peak at 561 cm^{-1} is attributed to the Sn–O signal (Fig. 1e), while the signals at 1089 and 1047 cm^{-1} are assigned to the P═O and P–O signals (Fig. 1f) in IL MPIMPH, respectively. Upon the introduction of the sample containing SnO_2, the P═O and P–O signals shift to 1086 and 1044 cm^{-1}, respectively, providing further evidence of the strong

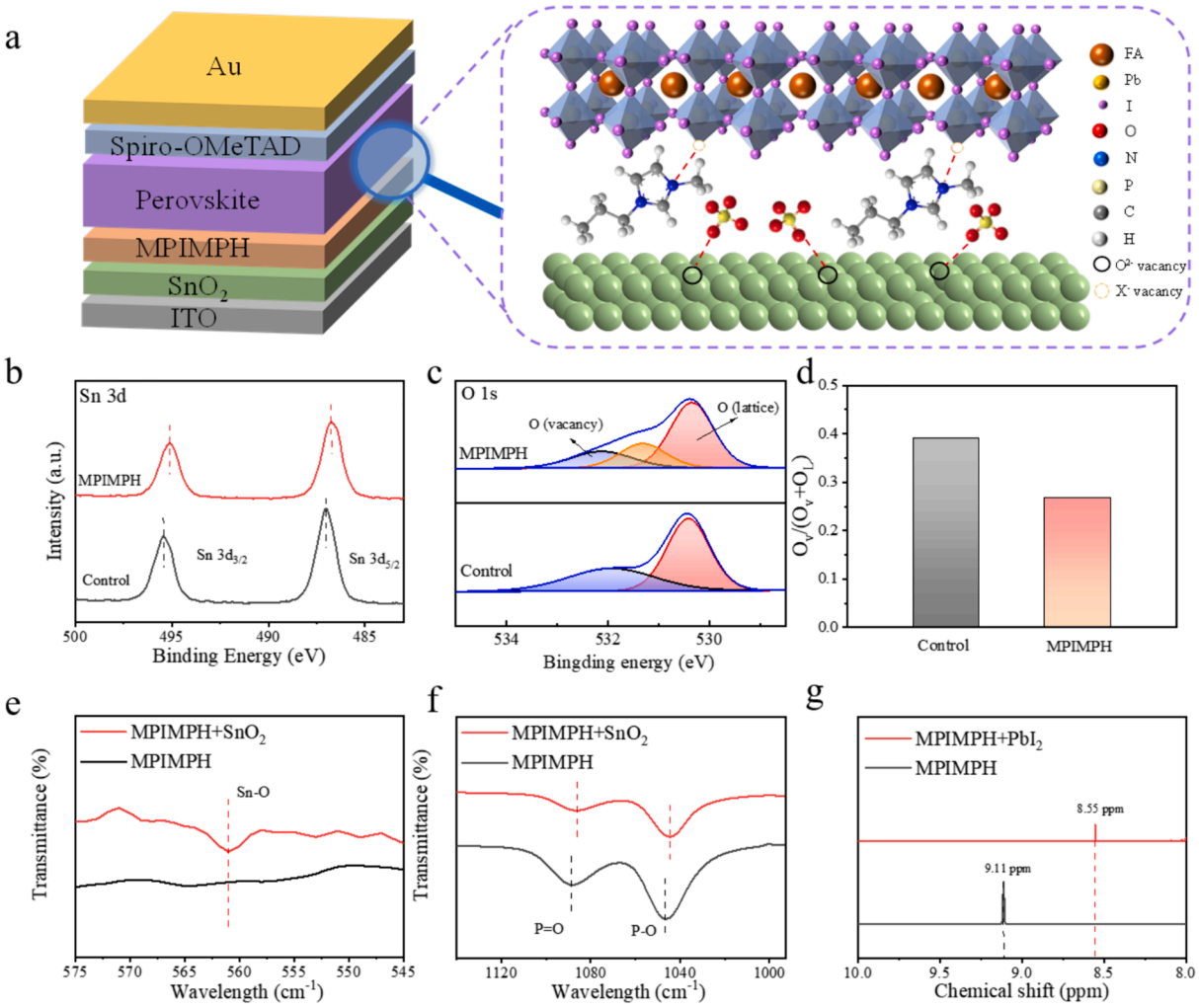

Fig. 1. (a) Schematic representation of the chemical interactions between ILs with SnO_2 and perovskite. XPS spectrum of (b) Sn 3d and (c) O 1s core levels of the control and IL-modified SnO_2 film. (d) The statistical ratio of oxygen vacancies (Ov) is derived from the calculation of the O 1s XPS spectrum. (e and f) FTIR spectrum of MPIMPH and MPIMPH + SnO_2 samples. (g) ^{1}H NMR spectrum of MPIMPH and MPIMPH + PbI_2 samples.

interaction between the phosphate groups in the IL MPIMPH and SnO_2. In addition to the previously mentioned interactions involving ILs and tin dioxide, NMR measurements were utilized to confirm the interactions between ILs and perovskite, as depicted in Fig. 1g and Fig. S3. Chemical shifts from 9.11 to 8.55 ppm in the resonance peaks of the imidazole group upon the adding PbI_2 to the MPIMPH solution indicate a strong interaction between imidazole groups and uncoordinated Pb^{2+}. Ultraviolet photoelectron spectroscopy (UPS) was employed to elucidate alterations in the conduction band (E_{CB}) position of SnO_2, showing positions for the pristine and IL MPIMPH-treated one as −4.32 eV and −4.24 eV, respectively (S4). The determination of valence band maximum (VBM) was carried out by the following formulas:

$$E_F = E_{cut\text{-}off} - 21.22$$

$$VBM = E_F - E_{onset}$$

for both control and MPIMPH-modified SnO_2 films, evidently observed values from UPS results for $E_{cut\text{-}off}$ and E_{onset} are 16.68 (16.88) eV and 3.78 (3.9) eV, respectively. Moreover, calculated VBM were −8.32 eV and −8.24 eV corresponding to the control and MPIMPH-modified SnO_2 films, respectively. Additionally, combining with the optical bandgap of SnO_2, perovskite and UPS spectrum of perovskite, we obtained energy level diagrams before and after modification (Fig. S5). These indicates that the conduction band of IL MPIMPH-modified SnO_2 closely approximates that of the perovskite, reducing interface energy barriers, suppressing of interface recombination, and enhancing of electron extraction efficiency. IL MPIMPH modification barely alters the transmittance of SnO_2 (Fig. S6).

With the aim of achieving a more comprehensive comprehension of the interactions between ILs and SnO_2 and elucidating the specific impact of the IL's chemical structure on its effectiveness in interacting with tin dioxide, while simultaneously providing specific evidence for the advantages of the chosen MPIMPH, a quantitative analysis was undertaken. First-principles DFT calculations were employed for this purpose (Fig. 2a). The detailed calculation method and constructed structure models are provided in Experimental Section for computational details and Fig. S7. The binding energies of frequently encountered anions in ILs with SnO_2 were calculated (Fig. 2b). The values for Br^-, Cl^-, I^-, Ac^-, BF_4^- and PO_4^{3-} were found to be −1.41, −1.98, −1.19, −3.31, −3.71 and −3.18 eV, respectively. A relatively higher binding energy indicates that, compared to traditional anions like Br^-, Cl^- and I^-, the anions Ac^-, BF_4^- and PO_4^{3-} exhibit stronger chemical interactions with SnO_2. The Sn vacancy formation energy of the above anions-modified SnO_2 film is also calculated (Fig. 2c). Phosphate ion treatment results in the highest energy required for tin vacancy formation in SnO_2 films. This observation underscores the optimal capacity of phosphate ions to efficiently inhibit the emergence of tin vacancies within the tin dioxide structure, leading to a substantial improvement in its charge transport capability.

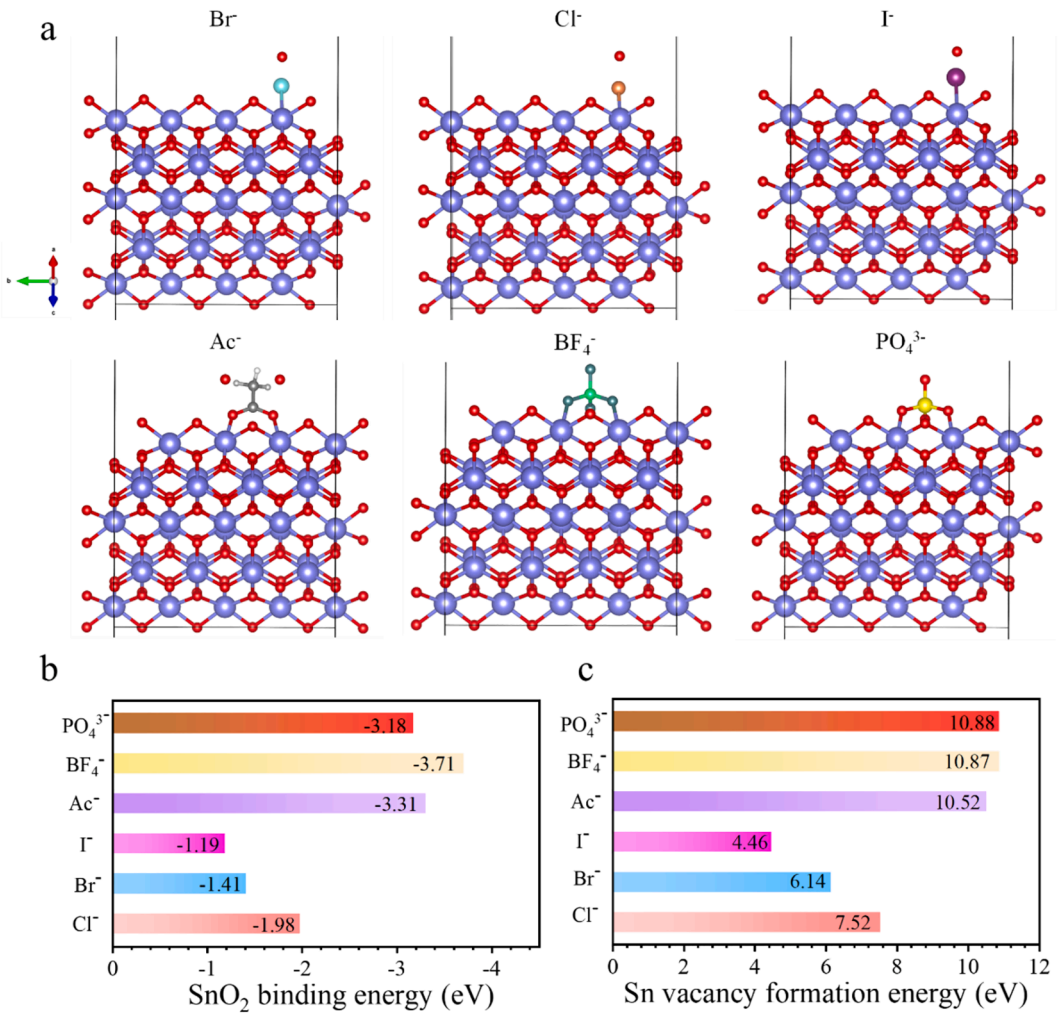

Fig. 2. (a) Optimized structures from the DFT calculations of Br^-, Cl^-, I^-, Ac^-, BF_4^- and PO_4^{3-}-modified SnO_2 surface. (b) The statistics of binding energy of SnO_2 with the above anions. (c) The statistics of Sn vacancy formation energy of the above anions-modified SnO_2 films.

To further investigate the impact of ILs interface modification on SnO_2, Atomic Force Microscopy (AFM) images of pristine and ILs-modified SnO_2 samples are obtained (Fig. 3a and b, Fig. S8). After modification with IL MPIMPH, the surface roughness of the film, measured as root-mean-squared (RMS) value, decreased slightly from 0.982 to 0.927 nm. This relatively improved surface smoothness indicates enhanced contact with the upper layer, thereby facilitating charge transport. Perovskite thin films were fabricated on SnO_2 and ILs-modified SnO_2 substrates using the traditional two-step method, and the corresponding SEM images of the perovskite films are shown in the Fig. 3c and d. In the control perovskite, a noticeable white substance is observed, while it is almost absent on the surface of the perovskite film modified with IL interface. In order to verify the white substance on the surface of the perovskite film in SEM, GIWAXS measurements have been performed. To specifically focus on the top surface of the perovskite thin film, we have varied the incident angle of X-ray to 0.1°. For the control sample, discernible scattering peak at $q = 9\ nm^{-1}$ can be seen, originated from large amount of PbI_2 residues on the top surface, while nearly no PbI_2 diffraction signal can be observed for MPIMPH-modified sample. It is reasonable to conclude that the while substance is PbI_2. AFM analyses were conducted for both control and ILs-modified perovskite films (Fig. S10). The improvement of film quality with larger grain size and less residual PbI_2 can be observed in ILs-modified perovskite film, which are entirely in line with those obtained from SEM images. Notably, a smoother and more level surface corresponding to the reduced roughness was demonstrated on the surface morphology of the ILs-modified perovskite film.Detailed 2D GIWAXS images are available in Fig. S9. In-situ UV–Vis absorption measurements were utilized during the thermal annealing process to investigate the effect of MPIMPH on the crystallization process of perovskite films (Fig. S11). For the control sample, a faster crystallization kinetics is monitored, along with the absorption intensity got stabilized after 55 s, while for MPIMPH-modified sample, a slower crystallization process is observed. It takes about 75 s to reach the stabilized absorption state. The introduction of MPIMPH has slowed down the perovskite crystallization kinetics, yielding relatively more time for the reaction between PbI_2 and organic salts, contributing to the conversion of PbI_2 into perovskite materials, which is consistent with the reduction of residual PbI_2 in SEM images. Excessive residual lead iodide can significantly compromise the device stability, and the effective management of lead iodide is crucial for the photovoltaic performance of the device [6,43]. Importantly, IL MPIMPH-modified perovskite film exhibits a more uniform morphology and larger average grain size (857 nm), significantly larger than the counterpart of the reference sample's 340 nm (Fig. 3e and f). In order to thoroughly elucidate the specific reasons for the enlargement of perovskite grains, contact angle tests were conducted for both control and MPIMPH-modified SnO_2 samples (Fig. S12). Compared to the 45° contact angle obtained from the control SnO_2 sample, the MPIMPH-modified SnO_2 sample exhibited a smaller contact angle (21°), indicative of lower surface energy. This lower surface energy facilitated the generation of larger perovskite grains [44]. To elucidate the significant role of PO_4^{3-} in shaping the morphology of perovskite films, SEM

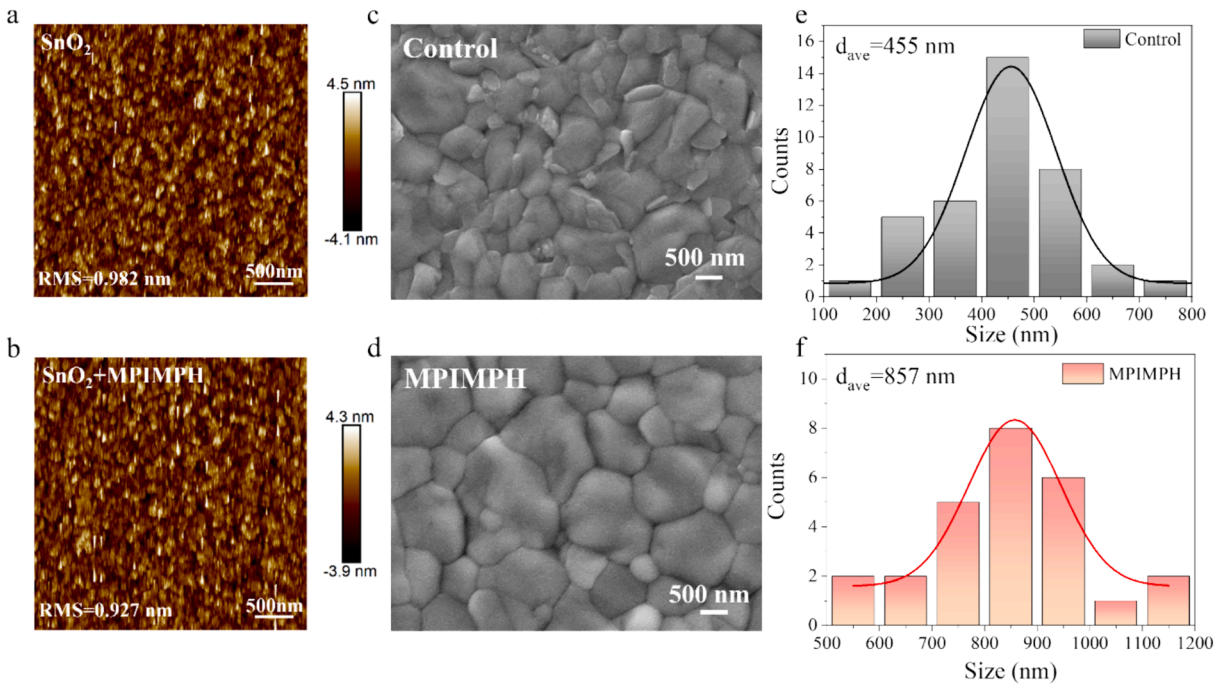

Fig. 3. AFM images of (a) control SnO_2 film and (b) MPIMPH-modified SnO_2 film. SEM images of (c) control perovskite film and (d) MPIMPH-modified perovskite film. (e and f) Corresponding statistics of particle size accroding to the SEM results.

measurements were conducted for the ILs with different anions (BF_4^-, I^-, Br^-, Cl^- and Ac^-) paired with the same cation (Fig. S13). Compared to the reference, SnO_2/perovskite modified with $MPIMBF_4$, MPIMI, MPIMBr, MPIMCl and MPIMAc exhibit higher film quality with larger grain size and less PbI_2 residues, as confirmed by grain size statistics. It is evident that ionic liquids containing $MPIM^+$ can effectively regulate the crystallization process of perovskite; however, the influence of different anions varies significantly. Owing to the presence of PO_4^{3-}, MPIMPH-modified perovskite film displays the largest grain size. The high quality perovskite film effectively reduces the number of grain boundaries, thereby mitigates non-radiative recombination. Therefore, the buried interface modification with ILs also plays a positive role in regulating the crystallization and morphology of perovskite.

X-ray diffraction (XRD) patterns were collected for both the unmodified and MPIMPH-modified perovskite films, aiming to comprehensively understand the influence of ILs' buried interface modification on the perovskite films. A consistent diffraction peak at 14.02°, aligned with the (1 1 0) crystal plane of perovskite, is evident in both the unmodified and MPIMPH-modified perovskite films (Fig. 4a). This suggests that the inclusion of ILs has minimal impact on perovskite structure in terms of polymorphism or lattice variation. Importantly, the intensity of the PbI_2 peak signal at 12.70° is significantly diminished in MPIMPH-modified films compared to the control film, indicating the effective decrease of PbI_2 residue following the buried interface modification through ILs. To further explore the impact of ILs, specifically MPIMPH, in promoting perovskite formation, systematic GIWAXS analysis was conducted. Fig. 4b and c presents the 2D GIWAXS patterns of both unmodified and MPIMPH-modified perovskite samples, the q_z points in the out-of-pane direction with respect to the sample surface and the q_{xy} represents the in-plane direction, respectively, the symmetry of the fiber texture can be used here to examine the scattering distribution in a single frame [44], displaying two scattering peaks located at $q = 9$ and 10 nm^{-1}, corresponding to the (1 1 0) planes of PbI_2 and the (1 1 0) planes of 3D perovskite crystals. Radial integration results (Fig. 3d) show a weaker PbI_2 signal in MPIMPH-modified perovskite samples, indicating that buried interface modification *via* ILs facilitates the conversion of PbI_2 into perovskite. Subsequent UV–Vis (Fig. 4e) and PL tests (Fig. 4f) were carried out on the perovskite films deposited onto both pristine and IL MPIMPH-modified SnO_2 film substrates. These tests exhibited nearly identical absorption thresholds and photoluminescence peak positions, signifying the preservation of the lattice structure, consistent with the XRD results. Simultaneously, the PL intensity and carrier lifetime of perovskite films utilizing ILs MPIMPH-modified ETLs demonstrated a notable decrease, which is due to the significant passivation effect of MPIMPH on defects in SnO_2, thereby promoting the extraction of more electrons from perovskit layer to the ETL with less recombination loss at ETL/perovskite interface (Fig. 4f and g) [45,46]. The corresponding decay parameters which are obtained by fitting the data with a bi-exponential decay function listed in Table S1, and the function is as follow:

$$f(x) = A_1 e^{\left(-\frac{x}{\tau 1}\right)} + A_2 e^{\left(-\frac{x}{\tau 2}\right)}$$

where A is the corresponding decay amplitude, τ_1 and τ_2 are the fast and slow decay times, respectively, and C is a constant. Additionally, the PL and time-resolved photoluminescence (TRPL) datas of perovskite films deposited on control and IL MPIMPH-modified glass substrates are also obtained in Fig. 4h and i. Similarly, we employed the above function to fit the data, demonstrating that a slower decay was observed in MPIMPH-modified perovskite films, associated with the improved quality of films (Table S2). Following the interface modification with IL MPIMPH on glass substrates, a notable enhancement is observed in both the PL intensity and acculated charge-carrier lifetime, further accentuating the role of ILs in mitigating defects at the bottom of the perovskite layer, reflecting in the suppression of interfacial charge recombination [47,48].

To gain a deeper understanding of the impact of ILs on device defects, we conducted space-charge limited current (SCLC) measurements, as depicted in Fig. 5a and b, and determined trap density using a previously reported formula. The flat-band voltage (V_{TFL}) diminishes from 0.269 to 0.153 V following the modification with MPIMPH, indicating a reduction in trap density (N_t) of the MPIMPH-modified film, reducing from 4.52×10^{15} to 2.42×10^{15} cm^{-3} (Fig. 5c). The reduced defect density indicates that ILs modification optimizes the formation of

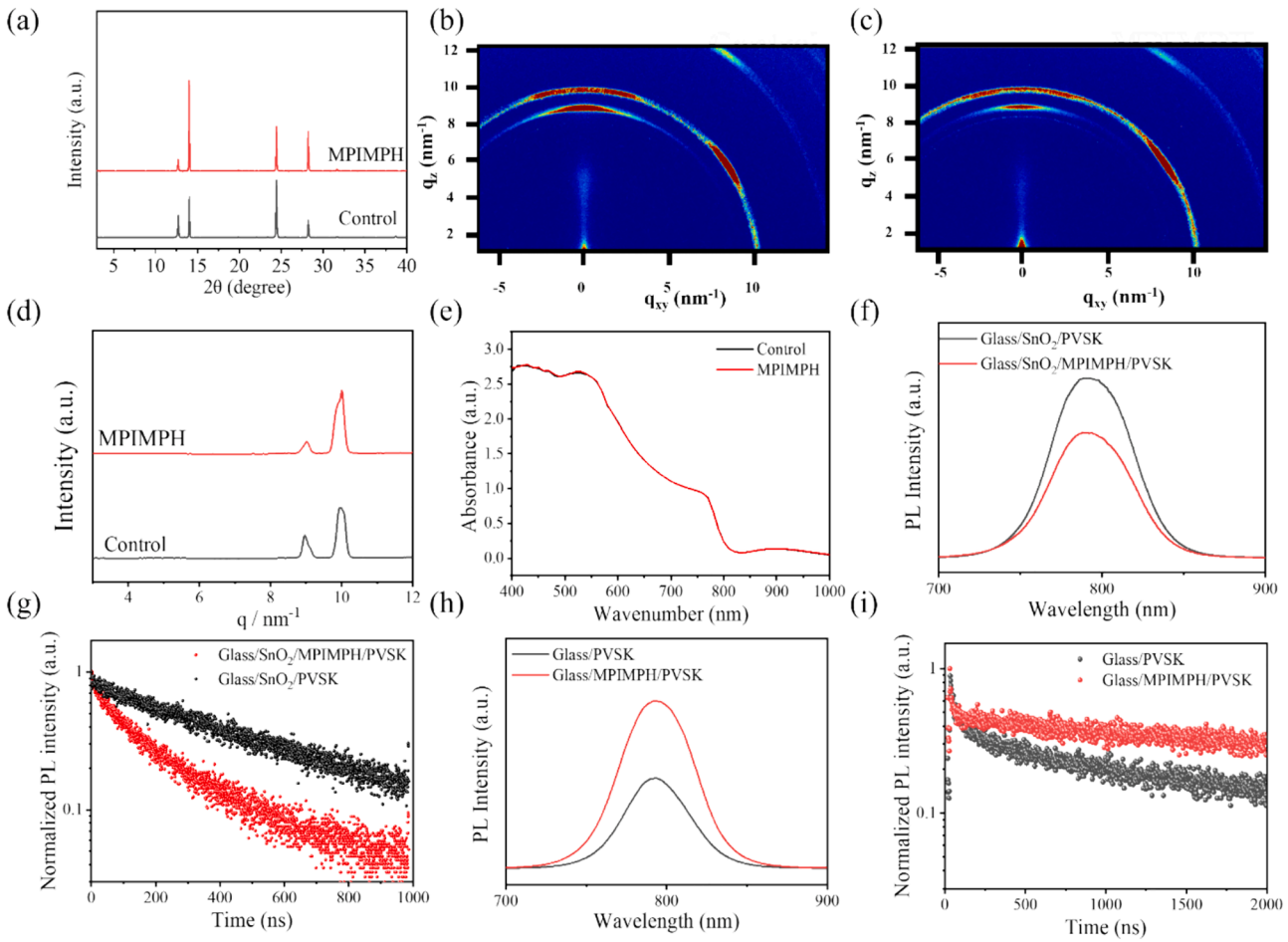

Fig. 4. (a) XRD data of perovskite films deposited on control and IL MPIMPH-modified SnO_2 film. (b and c) The 2D GIWAXS datas of perovskite films deposited on the control and IL MPIMPH-modified SnO_2 films. (d) The integrated datas from 2D GIWAXS patterns. (e) The UV–vis spectra of perovskite films deposited on control and IL MPIMPH-modified SnO_2 film. (f) PL and (g) TRPL datas of the perovskite films deposited on control and IL MPIMPH-modified SnO_2 film substrates. (h) PL and (i) TRPL datas of the perovskite films deposited on control and IL MPIMPH-modified glass substrates.

defects at perovskite grain boundaries and SnO_2/perovskite interface. To investigate the impact of buried interface modification with ILs on device performance, we varied the concentrations of MPIMPH to find the optimal level. The resulting champion PCE and associated photovoltaic parameters are presented in Fig. S14 and Table S3. Noticeable improvements in both *Voc* and FF are evident, attributed to the enhanced quality of perovskite films quality, with larger grain size, less residual PbI_2 and efficient passivation of defects. The device subjected to MPIMPH treatment achieved an elevated power conversion efficiency (PCE) of 24.24 %, characterized by an open-circuit voltage (*Voc*) of 1.185 V, a short-circuit current density (*Jsc*) of 25.18 mA cm^{-2}, and a fill factor (FF) of 81.25 %. In contrast, the top-performing pristine device exhibited a standard PCE of 22.60 %, accompanied by a *Voc* of 1.131 V, *Jsc* of 25.12 mA cm^{-2}, and FF of 79.55 % (Fig. 5d). Meanwhile, *J-V* curves tests were also employed to evaluate the photovoltaic performance of different ILs-modified PSCs, with specific *J-V* curves and photovoltaic parameters shown in Fig. S15 and Table S4. The PSCs treated with the five different ionic liquids (MPIMAc, $MPIMBF_4$, MPIMCl, MPIMBr and MPIMI) achieved champion efficiencies of 23.78 %,23.58 %, 23.13 %, 23.12 % and 23.10 %, respectively.The EQE spectra of the winning device using MPIMPH exhibit a closely matched integrated *Jsc* when compared with the *Jsc* measured from the *J-V* curve (Fig. 5e). To better illustrate the performance improvement of ILs for the device, hysteresis characteristics were demonstrated for both control and MPIMPH-modified PSCs in Fig. S16, and corresponding parameters were summarized in Table S4. Remarkably, introducing MPIMPH significantly reduced the hysteresis index (HI) from 0.108 to 0.066, owing to the reduction of SnO_2/perovskite interface defects and the inhibition of perovskite ion migration. Simultaneously, the statistical outcomes for performance parameters of MPIMPH-modified PSCs with an average PCE of 23.45 % also indicate a significant enhancement in reproducibility (Fig. 5f and Fig. S17). The steady-state PCE of control and MPIMPH-modified PSCs *via* maximum power point tracking are assessed in Fig. 5g, which demonstrated remarkable stability at 22.29 % and 23.97 %, respectively. These results align notably with the observations from the *J-V* curves. In Fig. 5d, the results of maximum power point (MPP) tracking are illustrated for both the control devices and those modified with MPIMPH. Even after 1000 h of continuous MPP tracking, the MPIMPH-modified device retains 91.2 % of its initial PCE, in contrast to the control device which drops below 85.3 %. The humidity stability of devices were subjected to testing, revealing that even after 1000 h of storage under a relative humidity of 40 %, the efficiency of the devices modified with IL MPIMPH managed to retain 90.1 % of their initial efficiency (Fig. S18). To comprehensively demonstrate the enhanced stability of MPIMPH-modified PSCs, cross-sectional SEM was utilized to monitor the evolution of perovskite layers (Fig. S19). After exposure to an environment of 25 °C, 40 % RH for 15 days, poor stability can be observed for the control device, characterized by incomplete grains and the precipitation of a large amount of PbI_2. In contrast, the perovskite layer of MPIMPH-modified PSCs remained stable. To investigate the effect of MPIMPH on the thermal stability of devices, we captured cross-sectional SEM images of both control and MPIMPH-

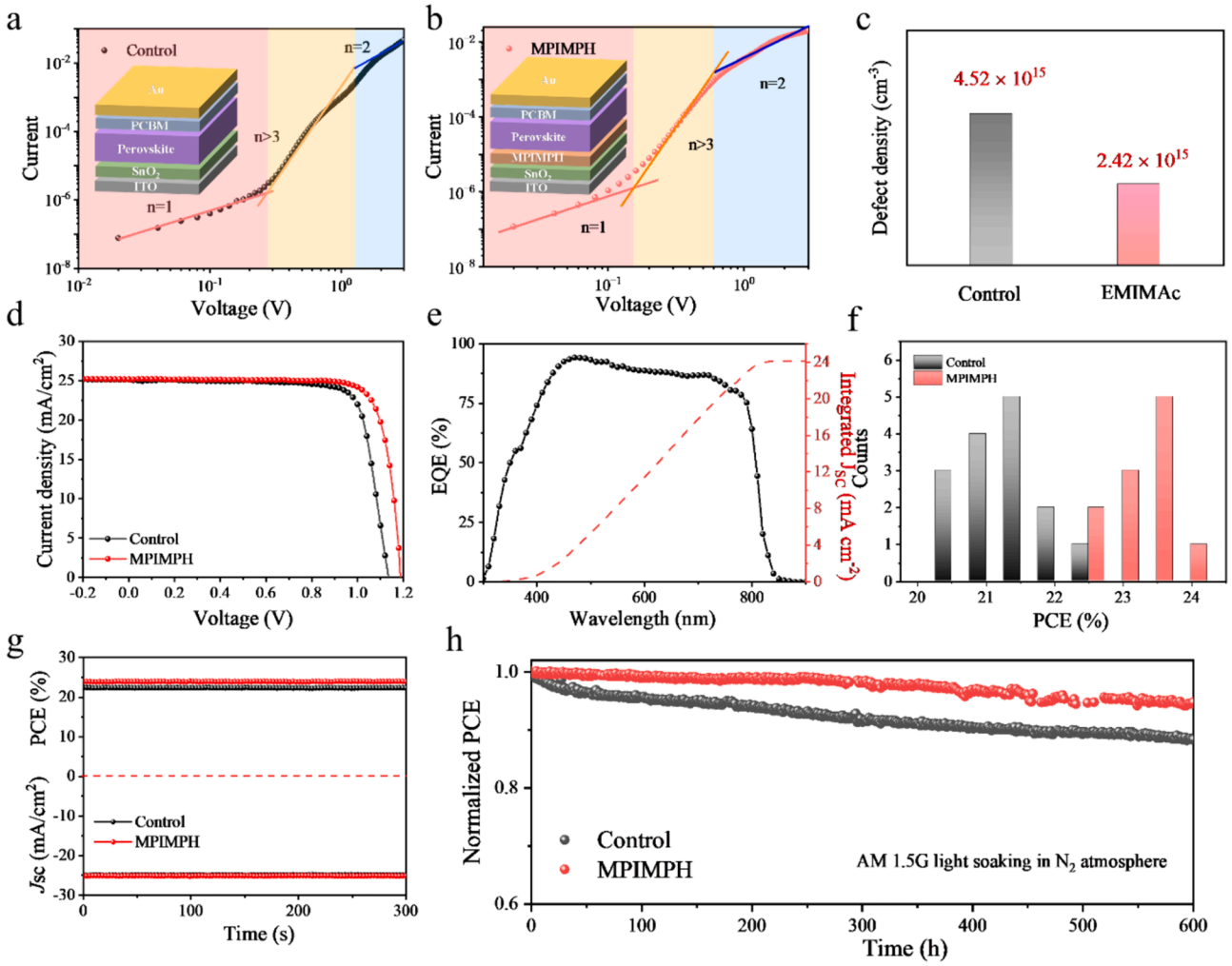

Fig. 5. (a and b) SCLC measurements of devices with the ITO/SnO_2 or SnO_2/MPIMPH/Perovskite/PCBM/Au. (c) Statistics of defect density calculated by SCLC measurements. (d) *J–V* characteristics of control and MPIMPH-modified PSCs. (e) EQE spectra of MPIMPH-modified PSCs. (f) The histogram of PCE for control and MPIMPH-modified devices. (g) Stability maximum power point for the control and MPIMPH-modified devices. (h) Stability of PSCs under MPP tracking with continuous illumination of AM 1.5G light soaking in N_2 atmosphere.

modified before and after heating in a 60 °C, 50 % RH environment. Upon substantial heating, the perovskite grains in the control sample were significantly damaged, with more occurrences of PbI_2, while the MPIMPH-modified exhibited only slight changes.

3. Conclusion

In this study, we employ IL MPIMPH, with phosphate (PO_4^{3-}) groups, as an interface modifier for SnO_2/perovskite interfaces and conduct comprehensive investigations to analyze the specific impact of IL MPIMPH on tin dioxide defects, perovskite defects, perovskite crystallization, morphology, and the overall device performance. Density Functional Theory (DFT) calculations are initially utilized to comprehensively assess the defect passivation potential of various anions on tin vacancies within the SnO_2 matrix. The results unequivocally highlight the exceptional defect passivation capabilities of the PO_4^{3-} group, distinguishing it from the numerous common anions (Br^-, Cl^-, I^-, Ac^- and BF_4^-). Substantial chemical interactions are confirmed between IL MPIMPH and both SnO_2 and perovskite, forming a fundamental basis for interface defect passivation. Furthermore, IL-based interface modification enhances interface contact, influencing the extent of lead iodide conversion into perovskite and perovskite crystallization, ultimately resulting in the production of high-quality perovskite thin films. The contribution on efficiently inhibiting interfacial charge recombination and fine-tuning the energy alignment at the SnO_2/perovskite interface, thereby improving carrier extraction has also been confirmed. Thanks to the interface modification with ILs, the optimized device achieves an impressive device efficiency of 24.24 % and demonstrates exceptional durability.

CRediT authorship contribution statement

Guo Yang: Writing – original draft, Software, Investigation, Data curation, Conceptualization. **Fei Wang:** Writing – review & editing, Software, Investigation, Formal analysis, Data curation. **Chao Zhou:** Software, Resources, Methodology, Data curation. **Yonggui Sun:** Software, Methodology, Data curation, Conceptualization. **Taomiao Wang:** Validation, Resources. **Qiannan Li:** Visualization, Formal analysis. **Yongjun Li:** Validation, Formal analysis. **Xiao Liang:** Software, Conceptualization. **Xianfang Zhou:** Resources, Data curation. **Quanyao Zhu:** Supervision, Project administration, Formal analysis. **Haoran Lin:** Supervision, Methodology, Conceptualization. **Hanlin Hu:** Writing – review & editing, Supervision, Project administration, Funding acquisition, Formal analysis.

Declaration of competing interest

The authors declare that they have no known competing financial

interests or personal relationships that could have appeared to influence the work reported in this paper.

Data availability

The authors do not have permission to share data.

Acknowledgements

This work is supported by the Scientific Research Startup Fund for Shenzhen High-Caliber Personnel of Shenzhen Polytechnic, No. 6022310038k. The financial support from Guangdong Basic and Applied Basic Research Foundation (No. 2023A1515011677), Shenzhen Science and Technology Innovation Commission (Project No. 20220811205532001) is gratefully acknowledged.

Appendix A. Supplementary data

Supplementary data to this article can be found online at https://doi.org/10.1016/j.cej.2024.152559.

References

[1] Z. Liu, F. Cao, M. Wang, M. Wang, L. Li, Observing defect passivation of the grain boundary with 2-aminoterephthalic acid for efficient and stable perovskite solar cells, Angew. Chem. - Int. Ed. 59 (2020) 4161–4167, https://doi.org/10.1002/anie.201915422.

[2] N. Li, X. Niu, L. Li, H. Wang, Z. Huang, Y. Zhang, Y. Chen, X. Zhang, C. Zhu, H. Zai, Y. Bai, S. Ma, H. Liu, X. Liu, Z. Guo, G. Liu, R. Fan, H. Chen, J. Wang, Y. Lun, X. Wang, J. Hong, H. Xie, D.S. Jakob, X.G. Xu, Q. Chen, H. Zhou, Liquid medium annealing for fabricating durable perovskite solar cells with improved reproducibility, Science (80-.) 373 (2021) 561–567, https://doi.org/10.1126/science.abh3884.

[3] H. Wang, F. Ye, J. Liang, Y. Liu, X. Hu, S. Zhou, C. Chen, W. Ke, C. Tao, G. Fang, Pre-annealing treatment for high-efficiency perovskite solar cells via sequential deposition, Joule 6 (2022) 2869–2884, https://doi.org/10.1016/j.joule.2022.10.001.

[4] X. Zhu, C. Wang, C. Zhang, Z. Wang, J. Feng, S. (Frank) Liu, D. Yang, Imidazolium-based ionic liquid for stable and highly efficient black-phase formamidinium-based perovskite solar cell, Chem. Eng. J. 434 (2022) 134759, https://doi.org/10.1016/j.cej.2022.134759.

[5] X. Zhou, Y. Wang, C. Li, T. Wu, Doping amino-functionalized ionic liquid in perovskite crystal for enhancing performances of hole-conductor free solar cells with carbon electrode, Chem. Eng. J. 372 (2019) 46–52, https://doi.org/10.1016/j.cej.2019.04.099.

[6] Y. Zhao, F. Ma, Z. Qu, S. Yu, T. Shen, H.-X. Deng, X. Chu, X. Peng, Y. Yuan, X. Zhang, J. You, Inactive (PbI 2) 2 RbCl stabilizes perovskite films for efficient solar cells, Science (80-.) 377 (2022) 531–534, https://doi.org/10.1126/science.abp8873.

[7] K. Deng, Q. Chen, L. Li, Modification engineering in SnO2 electron transport layer toward perovskite solar cells: efficiency and stability, Adv. Funct. Mater. 30 (2020) 1–16, https://doi.org/10.1002/adfm.202004209.

[8] C. Altinkaya, E. Aydin, E. Ugur, F.H. Isikgor, A.S. Subbiah, M. De Bastiani, J. Liu, A. Babayigit, T.G. Allen, F. Laquai, A. Yildiz, S. De Wolf, Tin oxide electron-selective layers for efficient, stable, and scalable perovskite solar cells, Adv. Mater. 33 (2021) 1–32, https://doi.org/10.1002/adma.202005504.

[9] M. Shahiduzzaman, E.Y. Muslih, A.K.M. Hasan, L. Le Wang, S. Fukaya, M. Nakano, M. Karakawa, K. Takahashi, M. Akhtaruzzaman, J.M. Nunzi, T. Taima, The benefits of ionic liquids for the fabrication of efficient and stable perovskite photovoltaics, Chem. Eng. J. 411 (2021) 128461, https://doi.org/10.1016/j.cej.2021.128461.

[10] D. Yang, X. Zhou, R. Yang, Z. Yang, W. Yu, X. Wang, C. Li, S. Liu, R.P.H. Chang, Surface optimization to eliminate hysteresis for record efficiency planar perovskite solar cells, Energ. Environ. Sci. 9 (2016) 3071–3078, https://doi.org/10.1039/c6ee02139e.

[11] D. Liu, S. Li, P. Zhang, Y. Wang, R. Zhang, H. Sarvari, F. Wang, J. Wu, Z. Wang, Z. D. Chen, Efficient planar heterojunction perovskite solar cells with Li-doped compact TiO2 layer, Nano Energy 31 (2017) 462–468, https://doi.org/10.1016/j.nanoen.2016.11.028.

[12] X. Huo, Y. Jiang, J. Lv, W. Sun, W. Liu, R. Yin, Y. Gao, K. Wang, T. You, P. Yin, Bottom-up multi-interface modification boosts the performance of carbon-based HTL-free all-inorganic CsPbI2Br perovskite solar cells, Chem. Eng. J. 484 (2024) 149626, https://doi.org/10.1016/j.cej.2024.149626.

[13] S. Zhang, H. Si, W. Fan, M. Shi, M. Li, C. Xu, Z. Zhang, Q. Liao, A. Sattar, Z. Kang, Y. Zhang, Graphdiyne: bridging SnO2 and perovskite in planar solar cells, Angew. Chem. - Int. Ed. 59 (2020) 11573–11582, https://doi.org/10.1002/anie.202003502.

[14] Q. Jiang, X. Zhang, J. You, SnO2: a wonderful electron transport layer for perovskite solar cells, Small 14 (2018) 1–14, https://doi.org/10.1002/smll.201801154.

[15] J. Chen, H. Dong, J. Li, X. Zhu, J. Xu, F. Pan, R. Xu, J. Xi, B. Jiao, X. Hou, K. Wei Ng, S.P. Wang, Z. Wu, Solar cell efficiency exceeding 25% through Rb-based perovskitoid scaffold stabilizing the buried perovskite surface, ACS Energy Lett. 7 (2022) 3685–3694, https://doi.org/10.1021/acsenergylett.2c01661.

[16] J. Du, L. Feng, X. Guo, X. Huang, Z. Lin, J. Su, Z. Hu, J. Zhang, J. Chang, Y. Hao, Enhanced efficiency and stability of planar perovskite solar cells by introducing amino acid to SnO2/perovskite interface, J. Power Sources 455 (2020) 227974, https://doi.org/10.1016/j.jpowsour.2020.227974.

[17] H. Min, D.Y. Lee, J. Kim, G. Kim, K.S. Lee, J. Kim, M.J. Paik, Y.K. Kim, K.S. Kim, M. G. Kim, T.J. Shin, S. Il Seok, Perovskite solar cells with atomically coherent interlayers on SnO2 electrodes, Nature 598 (2021) 444–450, https://doi.org/10.1038/s41586-021-03964-8.

[18] H. Zhang, S. Xu, T. Guo, D. Du, Y. Tao, L. Zhang, G. Liu, X. Chen, J. Ye, Z. Guo, H. Zheng, Dual effect of superhalogen ionic liquids ensures efficient carrier transport for highly efficient and stable perovskite solar cells, ACS Appl. Mater. Interfaces 14 (2022) 28826–28833, https://doi.org/10.1021/acsami.2c04993.

[19] E.H. Jung, B. Chen, K. Bertens, M. Vafaie, S. Teale, A. Proppe, Y. Hou, T. Zhu, C. Zheng, E.H. Sargent, Bifunctional surface engineering on SnO2reduces energy loss in perovskite solar cells, ACS Energy Lett. 5 (2020) 2796–2801, https://doi.org/10.1021/acsenergylett.0c01566.

[20] X. Guo, X. Huang, J. Su, Z. Lin, J. Ma, J. Chang, Y. Hao, Reducing the interfacial energy loss via oxide/perovskite heterojunction engineering for high efficient and stable perovskite solar cells, Chem. Eng. J. 417 (2021) 129184, https://doi.org/10.1016/j.cej.2021.129184.

[21] J. Chen, X. Zhao, S.G. Kim, N.G. Park, Multifunctional chemical linker imidazoleacetic acid hydrochloride for 21% efficient and stable planar perovskite solar cells, Adv. Mater. 31 (2019) 1–10, https://doi.org/10.1002/adma.201902902.

[22] Y. Li, S. Li, Y. Shen, X. Han, Y. Li, Y. Yu, M. Huang, X. Tao, Multifunctional histidine cross-linked interface toward efficient planar perovskite solar cells, ACS Appl. Mater. Interfaces 14 (2022) 47872–47881, https://doi.org/10.1021/acsami.2c13585.

[23] W. Fan, Y. Shen, K. Deng, Q. Chen, Y. Bai, L. Li, Synergistic bonding stabilized interface for perovskite solar cells with over 24% efficiency, Nano Energy 100 (2022) 107518, https://doi.org/10.1016/j.nanoen.2022.107518.

[24] S. You, H. Zeng, Z. Ku, X. Wang, Z. Wang, Y. Rong, Y. Zhao, X. Zheng, L. Luo, L. Li, S. Zhang, M. Li, X. Gao, X. Li, Multifunctional polymer-regulated SnO2 nanocrystals enhance interface contact for efficient and stable planar perovskite solar cells, Adv. Mater. 32 (2020) 1–10, https://doi.org/10.1002/adma.202003990.

[25] Q. Zhou, D. He, Q. Zhuang, B. Liu, R. Li, H. Li, Z. Zhang, H. Yang, P. Zhao, Y. He, Z. Zang, J. Chen, Revealing steric-hindrance-dependent buried interface defect passivation mechanism in efficient and stable perovskite solar cells with mitigated tensile stress, Adv. Funct. Mater. 32 (2022) 1–12, https://doi.org/10.1002/adfm.202205507.

[26] Y. Dong, W. Shen, W. Dong, C. Bai, J. Zhao, Y. Zhou, F. Huang, Y.B. Cheng, J. Zhong, Chlorobenzenesulfonic potassium salts as the efficient multifunctional passivator for the buried interface in regular perovskite solar cells, Adv. Energy Mater. 12 (2022) 1–12, https://doi.org/10.1002/aenm.202200417.

[27] Y. Du, Y. Wang, J. Wu, Q. Chen, C. Deng, R. Ji, L. Sun, L. Tan, X. Chen, Y. Xie, Y. Huang, Y. Vaynzof, P. Gao, W. Sun, Z. Lan, <scp> NaHCO $_3$ </scp> -induced porous <scp> PbI $_2$ </scp> enabling efficient and stable perovskite solar cells, InfoMat. 5 (2023), https://doi.org/10.1002/inf2.12431.

[28] X. Deng, L. Xie, S. Wang, C. Li, A. Wang, Y. Yuan, Z. Cao, Ionic liquids engineering for high-e ffi ciency and stable perovskite solar cells, Chem. Eng. J. 398 (2020) 125594, https://doi.org/10.1016/j.cej.2020.125594.

[29] F. Wang, T. Wang, Y. Sun, X. Liang, G. Yang, Q. Li, Y. Li, X. Zhou, Q. Zhu, A. Ng, H. Lin, M. Yuan, Y. Shi, T. Wu, H. Hu, Two-step perovskite solar cells with > 25% efficiency: unveiling the hidden bottom surface of perovskite layer, Adv. Mater. (2024) 2401476, https://doi.org/10.1002/adma.202401476.

[30] X. Shang, X. Ma, F. Meng, J. Ma, L. Yang, M. Li, D. Gao, C. Chen, Zwitterionic ionic liquid synergistically induces interfacial dipole formation and traps state passivation for high-performance perovskite solar cells, J. Colloid Interface Sci. 630 (2023) 155–163, https://doi.org/10.1016/j.jcis.2022.10.051.

[31] Z. Lin, X. Xu, H. Dong, Q. Song, H. Duan, C. Mu, Enhancing the efficiency of perovskite solar cells by bidirectional modification of the perovskite and electron transport layer, ACS Appl. Mater. Interfaces (2022), https://doi.org/10.1021/acsami.2c18341.

[32] F. Wang, K. Zhou, C. Zhou, X. Liang, T. Wang, Y. Sun, Y. Li, Q. Li, X. Zhou, G. Yang, D. Duan, J. Zhu, Q. Zhu, H. Lin, Y. Shi, C. Yang, G. Xing, H. Hu, Ionic liquid-induced 1D perovskite: exploring 1D perovskite structure to 1D/3D heterojunction-based photovoltaics, Adv. Energy Mater. (2024) 2400021, https://doi.org/10.1002/aenm.202400021.

[33] W. Zhang, X. Liu, B. He, Z. Gong, J. Zhu, Y. Ding, H. Chen, Q. Tang, Interface engineering of imidazolium ionic liquids toward efficient and stable CsPbBr 3 perovskite solar cells, ACS Appl. Mater. Interfaces 12 (2020) 4540–4548, https://doi.org/10.1021/acsami.9b20831.

[34] Z. He, S. Zhang, Y. Hu, Q. Geng, W. Zhao, D. Wang, Q. Tao, Q. Xu, M. Jiao, Synergistic enhancement of efficiency and stability of perovskite solar cells via dual interface modification, Appl. Surf. Sci. 611 (2023) 155745, https://doi.org/10.1016/j.apsusc.2022.155745.

[35] E. Jiang, Y. Ai, J. Yan, N. Li, L. Lin, Z. Wang, C. Shou, B. Yan, Y. Zeng, J. Sheng, J. Ye, Phosphate-passivated SnO2 electron transport layer for high-performance perovskite solar cells, ACS Appl. Mater. Interfaces 11 (2019) 36727–36734, https://doi.org/10.1021/acsami.9b11817.

[36] X. Sha, J. Sheng, W. Yang, J. Sun, C. Shou, L. Zhang, N. Zhang, Z. Ying, X. Yang, H. Zhao, J. Ye, Interfacial defect passivation by using diethyl phosphate salts for high-efficiency and stable perovskite solar cells, J. Mater. Chem. A 11 (2023) 6556–6564, https://doi.org/10.1039/d2ta09696j.
[37] X. Huang, J. Du, X. Guo, Z. Lin, J. Ma, J. Su, L. Feng, C. Zhang, J. Zhang, J. Chang, Y. Hao, Polyelectrolyte-doped SnO2 as a tunable electron transport layer for high-efficiency and stable perovskite solar cells, Sol. RRL 4 (2020) 1900336, https://doi.org/10.1002/solr.201900336.
[38] Q. Zhuang, C. Zhang, C. Gong, H. Li, H. Li, Z. Zhang, H. Yang, J. Chen, Z. Zang, Tailoring multifunctional anion modifiers to modulate interfacial chemical interactions for efficient and stable perovskite solar cells, Nano Energy 102 (2022) 107747, https://doi.org/10.1016/j.nanoen.2022.107747.
[39] X. Guo, J. Du, Z. Lin, J. Su, L. Feng, J. Zhang, Y. Hao, J. Chang, Enhanced efficiency and stability of planar perovskite solar cells using SnO2:InCl3 electron transport layer through synergetic doping and passivation approaches, Chem. Eng. J. 407 (2021) 127997, https://doi.org/10.1016/j.cej.2020.127997.
[40] S. Yang, W. Liu, Y. Han, Z. Liu, W. Zhao, C. Duan, Y. Che, H. Gu, Y. Li, S. Liu, 2D Cs2PbI2Cl2 nanosheets for holistic passivation of inorganic CsPbI2Br perovskite solar cells for improved efficiency and stability, Adv. Energy Mater. 10 (2020) 2002882, https://doi.org/10.1002/aenm.202002882.
[41] D. Zhao, C. Zhang, J. Ren, S. Li, Y. Wu, Q. Sun, Y. Hao, Buried interface optimization for flexible perovskite solar cells with high efficiency and mechanical stability, Small 2308364 (2023) 1–10, https://doi.org/10.1002/smll.202308364.
[42] L. Yang, J. Feng, Z. Liu, Y. Duan, S. Zhan, S. Yang, K. He, Y. Li, Y. Zhou, N. Yuan, J. Ding, S. Liu, Record-efficiency flexible perovskite solar cells enabled by multifunctional organic ions interface passivation, Adv. Mater. 34 (2022) 2201681, https://doi.org/10.1002/adma.202201681.
[43] X. Chen, J. Wu, G. Li, Y. Du, Q. Chen, C. Deng, Y. Xu, S. Zhu, F. Cai, J. Liu, Y. Wei, Y. Huang, Polarized molecule 4-(aminomethyl) benzonitrile hydrochloride for efficient and stable perovskite solar cells, ACS Appl. Mater. Interfaces (2022), https://doi.org/10.1021/acsami.2c09058.
[44] D. Yang, R. Yang, K. Wang, C. Wu, X. Zhu, J. Feng, X. Ren, G. Fang, S. Priya, S. (Frank) Liu, High efficiency planar-type perovskite solar cells with negligible hysteresis using EDTA-complexed SnO2, Nat. Commun. 9 (2018) 3239, https://doi.org/10.1038/s41467-018-05760-x.
[45] Y. Chen, X. Zuo, Y. He, F. Qian, S. Zuo, Y. Zhang, L. Liang, Z. Chen, K. Zhao, Z. Liu, J. Gou, S. Liu, Dual passivation of perovskite and SnO2 for high-efficiency MAPbI3 perovskite solar cells, Adv. Sci. 8 (2021) 1–8, https://doi.org/10.1002/advs.202001466.
[46] H. Dong, J. Wang, X. Li, W. Liu, T. Xia, D. Yao, L. Zhang, C. Zuo, L. Ding, F. Long, Modifying SnO2 with polyacrylamide to enhance the performance of perovskite solar cells, ACS Appl. Mater. Interfaces 14 (2022) 34143–34150, https://doi.org/10.1021/acsami.2c08662.
[47] L. Zhao, J. Gao, Y.H.L. Lin, Y.W. Yeh, K.M. Lee, N. Yao, Y.L. Loo, B.P. Rand, Electrical stress influences the efficiency of CH3NH3PbI3 perovskite light emitting devices, Adv. Mater. 29 (2017) 1–6, https://doi.org/10.1002/adma.201605317.
[48] G.H. Ahmed, J.K. El-Demellawi, J. Yin, J. Pan, D.B. Velusamy, M.N. Hedhili, E. Alarousu, O.M. Bakr, H.N. Alshareef, O.F. Mohammed, Giant photoluminescence enhancement in CsPbCl3 perovskite nanocrystals by simultaneous dual-surface passivation, ACS Energy Lett. 3 (2018) 2301–2307, https://doi.org/10.1021/acsenergylett.8b01441.